Tuning of spin relaxation and the Kondo effect in copper thin films by ionic gating

Xingyu Shen [1] Yunjiao Cai,[1] Yizheng Wu,[2,3] and Yi Ji[1,*]

[1]*Department of Physics and Astronomy, University of Delaware, Newark, Delaware 19716, USA*
[2]*Department of Physics, State Key Laboratory of Surface Physics, Fudan University, Shanghai 200433, People's Republic of China*
[3]*Shanghai Research Center for Quantum Sciences, Shanghai 201315, People's Republic of China*

Spin relaxation length is a fundamental material parameter that influences all aspects of spin dependent transport. The ability to tune the spin relaxation length leads to novel spintronic phenomena and functionalities. We explore the tunability of the spin relaxation length in the mesoscopic Cu channels of nonlocal spin valves by using the ionic gating technique via a Li^+ containing solid polymer electrolyte. At 5 K, the Cu spin relaxation length λ_{Cu} is tuned reversibly between 670 and 410 nm and the Cu resistivity ρ_{Cu} is tuned by 9%. The strength of the Kondo effect due to the Fe impurities in Cu is tuned by one order of magnitude. At 295 K, λ_{Cu} is tuned between 380 and 300 nm and ρ_{Cu} is tuned by 7%. A gradual amplification of the tuning ranges by repeated gate cycling is observed and clearly suggests an electrochemical origin. Tunable spin relaxation in simple metals enriches functionalities in metal-based spintronics and shines light on fundamental spin relaxation mechanisms.

I. INTRODUCTION

The research of spintronics has evolved rapidly to encompass a broad range of ideas and materials systems, some of which may lead to disruptive technologies for computer memory and logic, quantum information processing [1,2], and neuromorphic computing [3]. Many of the essential spintronic functionalities are carried by the spin current, which is a flow of electronic spin angular momentum. While a spin current is often accompanied by a charge current, a pure spin current without a net charge current can be generated as well. Two major challenges to the practicality of spin current are the lack of tunability and the ubiquitous spin relaxation. A tunable spin current has been desired since the inception of spintronics [4], but remains a major challenge despite some encouraging progress [5]. The spin relaxation occurs in all materials and results in an exponential decay of the injected spin current over distance. The characteristic decay length is known as the spin relaxation length λ. A short λ leads to a rapidly diminishing spin current that hinders the application potential.

Spin relaxation lengths in various materials span a broad range from a few nanometers [6] to exceeding 100 micrometers [7]. Achieving a long spin relaxation length is nontrivial: λ depends not only on the material itself but also on its crystallinity, dimensions, microstructures, and surface conditions. The exact factors that influence spin relaxation are yet fully understood. For a specific material in a given spin transport structure, however, the spin relaxation length is typically a fixed quantity. The prospect of a tunable spin relaxation length by an electric voltage is intriguing and naturally leads to a tunable spin current. In this manner, the spin current tunability

can be achieved by taking advantage of the spin relaxation processes occurring in all materials.

Two dimensional (2D) materials have been leading the way in gate tunable spin relaxation. Anisotropy in spin relaxation has been observed in graphene heterostructures [8,9] or bilayer graphene [10] and attributed to the spin-orbit effects. A gate voltage tunes the spin-orbit effects and thereby the spin relaxation [10]. In black phosphorous, the spin relaxation strongly depends on the carrier concentration, which can be modulated by an electrical gate [11]. Metallic materials, on the other hand, have not been explored for tunable spin relaxation, because their charge screening length is short and electric fields cannot influence the bulk of the metal. However, several metals, such as Cu, Ag, and Al, have substantial spin relaxation lengths and are desirable materials for spin transport channels [12–15]. One recent study shows an average λ of 2.6 μm at 30 K in submicron Cu channels [15]. Metallic materials also have the advantage of straightforward fabrication and being able to accommodate a much larger spin current than 2D materials. The capability of tuning the spin relaxation length on demand in metals will be a valuable addition.

In this work, we demonstrate that the spin relaxation length λ_{Cu}, the resistivity ρ_{Cu} and the Kondo effect in Cu thin films can be effectively tuned by using the ionic gating technique [16–23]. A polymer electrolyte, polyethylene oxide (PEO) and lithium perchlorate ($LiClO_4$), is applied between a metal gate and a submicron Cu-based nonlocal spin valve (NLSV) [13,24,25] as the gating medium [26]. At room temperature (RT), a positive (negative) gate voltage V_g induces an accumulation of Li^+ (ClO_4^-) ions on the surfaces of the NLSV. The electrolyte freezes below 273 K and low temperature gating is achieved by cooling the NLSV under a V_g from 295 K.

At 5 K, λ_{Cu} is tuned between 670 and 410 nm reversibly in a gated NLSV, resulting in the modulation of the nonlocal spin signal by a factor of 3. In addition, ρ_{Cu} is tuned by 8.7%

*yji@udel.edu
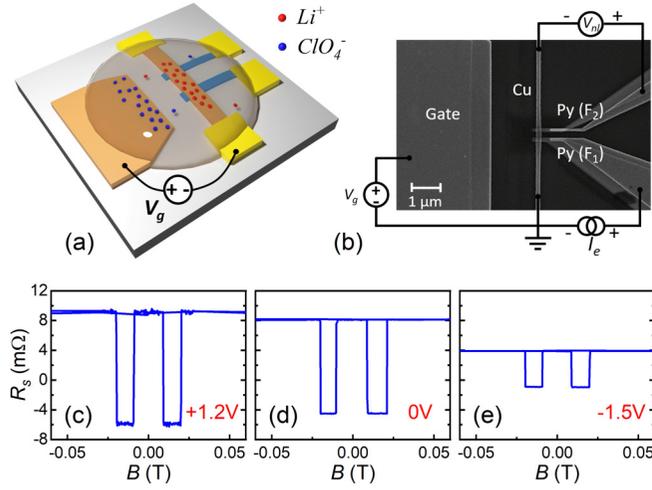
FIG. 1. (a) A cartoon illustration of ionic gating on a NLSV. (b) The SEM image of a NLSV with a side gate. R_s versus B curves of the NLSV device with $L = 800$ nm at 5 K after cooling the device from 295 K under V_g of (c) $+1.2$ V, (b) 0 V, and (c) -1.5 V.

and the strength of the Kondo effect is tuned by one order of magnitude. The tuning of ρ_{Cu} and λ_{Cu} has been achieved at RT as well, though the tuning ranges are smaller than those at 5 K. Upon repeated gate cycling, both λ_{Cu} and its tuning range gradually increase suggesting an electrochemical origin. We further hypothesize that Li ions/atoms diffuse into and out of the Cu channel along the grain boundaries under ionic gating and induce the observed tuning effects.

II. SAMPLE FABRICATION AND MEASUREMENT

Figure 1(a) is a cartoon illustration of the mesoscopic experimental structure and Fig. 1(b) is a scanning electron microscope (SEM) image of the structure before the ionic gel is applied. The key component of the structure is a metallic NLSV, which consists of a spin injector (F_1) and a spin detector (F_2), both ferromagnetic, as well as a nonmagnetic Cu channel. The spin relaxation process in Cu can be quantitatively investigated by using the NLSV. In Figs. 1(a) and 1(b), F_1 and F_2 are the pair of parallel stripes underneath the Cu channel and they are made of $Ni_{81}Fe_{19}$ alloy known as permalloy (Py). A 3-nm layer of AlO_x is placed between the Py stripes (F_1 and F_2) and the Cu channel to enhance the efficiency of spin injection and spin detection for F_1 and F_2, respectively [25,27]. In addition to the NLSV, a Cu gate electrode is patterned 2 or 5 μm away from the Cu channel for the ionic gating purpose. To fabricate the entire structure, electron beam lithography is used to create a mesoscopic shadow mask via two layers of electron beam resist on a Si substrate. Subsequently, Py is deposited from an oblique angle and AlO_x and Cu are deposited along the substrate normal direction through the shadow mask [25,27]. This angle deposition method ensures the pristine quality of the spin injection/detection interfaces $Py/AlO_x/Cu$ at F_1 and F_2, because they are formed without breaking the chamber vacuum.

The spin injection and detection method can be explained by referring the circuity in Fig. 1(b). An electric current I_e flows from F_1 toward the grounded end of the Cu channel and injects spin polarized electrons across the $F_1/AlO_x/Cu$ interface into Cu. A split between the spin-up and spin-down electrochemical potentials, also known as a spin accumulation, is induced in Cu but decays exponentially over distance due to the spin relaxation. The gradient of the spin accumulation drives diffusive spin currents toward both ends of the Cu channel. F_2 is used as a spin-dependent detector to probe the spin accumulation in Cu. A nonlocal voltage V_{nl} is measured between F_2 and the floating end of the Cu channel. The nonlocal resistance $R_s = V_{nl}/I_e$ is recorded as a function of a magnetic field B applied parallel to F_1 and F_2 stripes. Example R_s versus B curves are shown in Figs. 1(c)–1(e). As the B field is swept, parallel (P) and antiparallel (AP) alignments between the F_1 and F_2 magnetizations can be reached. The high values of R_s correspond to the P state and the low values to the AP state.

The difference between P and AP states is the spin signal ΔR_s and is proportional to the spin accumulation in the Cu channel at the location of F_2. Quantitatively, ΔR_s is given by [28]

$$\Delta R_s = \frac{P_1 P_2 \rho_{Cu} \lambda_{Cu}}{A} e^{-L/\lambda_{Cu}}, \tag{1}$$

where P_1 and P_2 are the effective spin polarizations of F_1 and F_2 across the $Py/AlO_x/Cu$ interfaces, respectively, L is the center-to-center distance between F_1 and F_2, and A is the cross-sectional area of the channel. It is common to assume $P_1 = P_2 = P_e$ when F_1 and F_2 have similar widths and thicknesses. As L increases, ΔR_s decreases exponentially with a characteristic decay length λ_{Cu} as expected with spin relaxation. A standard method of finding λ_{Cu} is to fit Eq. (1) to the data of ΔR_s versus L for a series of NLSVs with varying L. Alternatively, λ_{Cu} can also be directly calculated from the measured ΔR_s of a single NLSV by using Eq. (1) if P_e and ρ_{Cu} are known. Note that ρ_{Cu} can be measured directly on the NLSV by sending in a current through the Cu channel and measuring the voltage drop between F_1 and F_2.

The ionic gel of the electrolyte is prepared by mixing lithium perchlorate ($LiClO_4$) and polyethylene oxide (PEO) and then dissolving the mixture in methanol and deionized water at the proper ratio. A drop of the liquid is applied to the structure covering both the gate and the NLSV. The sample is left in air for 30 min for the methanol and water to evaporate and subsequently placed into the sample tube of a variable temperature cryostat. The sample tube is evacuated to vacuum and back filled with helium exchange gas at 295 K. Measurements can be conducted between 295 and 5 K.

As illustrated in Figs. 1(a) and 1(b), a voltage source connected between the gate and the Cu channel provides the gate voltage V_g. At RT, Li^+ and $ClO4^-$ ions are driven by V_g to move through PEO and accumulate on the negative and positive electrodes, respectively. Under a positive V_g, for example, Li^+ accumulate on the surfaces of the Cu channel as illustrated in Fig. 1(a). Upon electrolyte freezing below 273 K, the ion accumulation on the Cu surface cannot be altered by changing or removing V_g. The gating measurements at cryogenic temperatures are performed by setting the desired V_g at
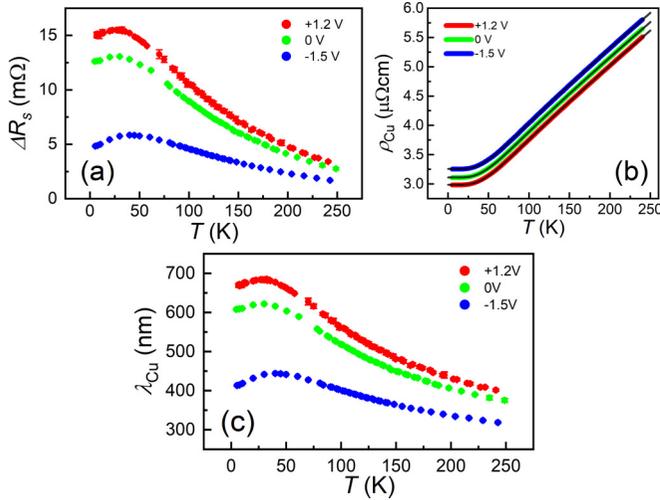
FIG. 2. (a) The spin signal and (b) the Cu resistivity as a function of T as the NLSV is cooled under various V_g. Solid lines in (b) are fits by using the Bloch-Grüneisen term for phonon resistivity. (c) Derived λ_{Cu} as functions of T under various V_g values.

FIG. 3. R_s versus B curves for a NLSV with an Al channel under V_g of (a) $+3.5$ V and (b) -3.5 V at 295 K. R_s versus B curves for the Cu-based device under V_g of (c) $+1.2$ V and (d) -1.5 V at 295 K.

295 K and cooling the device under this V_g to temperatures below 250 K. To reset V_g, the sample is first warmed up to 295 K before a different V_g can be effectively applied.

More than 10 NLSV devices have been measured and consistently show the tuning effects. In the following we focus on the data from one device, which has been measured for both ρ_{Cu} and λ_{Cu} at various temperatures under prolonged gate cycling. The Cu channel of this device has a cross sectional area of $A = 200 \times 65$ nm^2 with 200 nm being the width and 65 nm being the thickness. The length of the channel between the centers of F_1 and F_2 is $L = 800$ nm. The distance between the gate and the Cu channel is 5 μm.

III. LOW TEMPERATURE TUNING OF λ_{Cu} AND ρ_{Cu}

Here we describe the gating measurements at low temperatures, where the largest tuning of λ_{Cu} has been observed. The NLSV device is cooled from 295 to 5 K under three different V_g values of $+1.2$, 0, and -1.5 V, and distinctly different ΔR_s values of 15, 13, and 5 mΩ, respectively, are measured at 5 K as shown in Figs. 1(c) through 1(e). While the positive V_g results in a larger ΔR_s, the negative V_g leads to a smaller ΔR_s that is only 1/3 of the former. Such a dramatic change of spin signal in the same NLSV is striking. The change can be reversed by warming up the device to 295 K and cooling down under the opposite V_g. ΔR_s as a function of T between 5 and 250 K has been measured and shown in Fig. 2(a) for the three V_g values, and clearly the differences in ΔR_s are maintained at all temperatures. The unusual decease of ΔR_s at lower T (<40 K) is a well-documented sign of the enhanced spin relaxation by the Kondo effect [15,29,30].

The tuning of ΔR_s arises primarily from the tuning of λ_{Cu} as justified in the following. In Eq. (1) ΔR_s is related to a few parameters. While L and A are geometrical and are unlikely to be affected by the gating, a change in ΔR_s may be potentially traced to the changes in P_e, λ_{Cu}, or ρ_{Cu}. P_e is determined by the intrinsic polarization of Py as well as the Py/AlO$_x$/Cu in-

terfaces. λ_{Cu} and ρ_{Cu} reflect the properties of the Cu channel. The Py electrodes and the Py/AlO$_x$/Cu interfaces are unlikely affected by the gating because they are buried underneath the 65-nm-thick Cu channel. To illustrate this point further, we perform gating measurements on NLSVs which have 65-nm-thick Al channels but are otherwise similar to the Cu-based NLSVs. Despite applied V_g up to 3.5 V in both polarities, no tuning of ΔR_s or ρ_{Al} has been observed. The spin signals from one of the Al-based NLSVs, shown in Figs. 3(a) and 3(b), are $\Delta R_s = 4.0$ mΩ under both $V_g = +3.5$ V and $V_g = -3.5$ V at 295 K. This illustrates that the ionic gating cannot directly tune P_e by affecting the Py film or the Py/AlO$_x$ interface through a 65-nm nonmagnetic film.
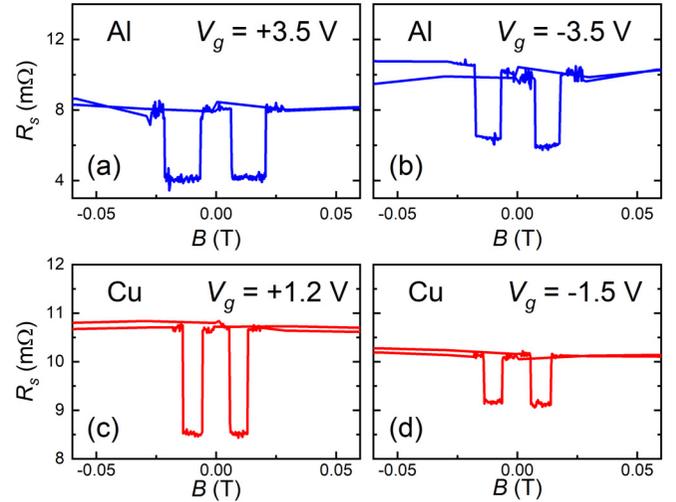
In contrast, the spin signals for the Cu-based device under opposite V_g values are clearly different even at 295 K, as shown in Figs. 3(c) and 3(d). $\Delta R_s = 2.2$ mΩ under $V_g = +1.2$ V and $\Delta R_s = 1.0$ mΩ under $V_g = -1.5$ V. This gate-induced change in ΔR_s should primarily come from the tuning of Cu properties (λ_{Cu} and ρ_{Cu}). When $|V_g| > 2.0$ V is applied to the Cu channels, irreversible electrochemical changes usually occur. Both Al and Cu channels are covered by natural oxides. The oxide on Al is more uniform and we will discuss in Sec. VI why ionic gating has no effect on the Al properties (λ_{Al} and ρ_{Al}) at all.

The Cu resistivity ρ_{Cu} versus T under various V_g values is directly measured and shown in Fig. 2(b). Indeed ρ_{Cu} is tuned by V_g. At 5 K, the value of ρ_{Cu} under $V_g = +1.2$ V is 9% lower than that under $V_g = -1.5$ V. To derive the tuning of λ_{Cu}, we assume that $P_e = P_0(1 - \alpha T^{3/2})$, where P_0 is the polarization at $T = 0$. This relation is based on the assumption that P_e scales with the Py magnetization which follows a temperature dependence that is well documented in the literature [31–33]. From our previous data [25,34] on Py/AlO$_x$/Cu NLSVs and taking into account the dimensions of the current device, we estimate $P_0 = 0.18$ and $P_e = 0.10$ at 295 K yielding $\alpha = 8.77 \times 10^{-5}$ K$^{-3/2}$. By using Eq. (1), the relations of λ_{Cu} versus T under various V_g, shown in Fig. 2(c), are derived from the data of ΔR_s versus T in Fig. 2(a), ρ_{Cu} versus T in

TABLE I. The ρ_{Cu} and λ_{Cu} of the NLSV device under various V_g values at 5 and 295 K. The percentage change is relative to the value under $V_g = 0$.

	ρ_{Cu} ($\mu\Omega$ cm) at 5 K	λ_{Cu} (nm) at 5 K	ρ_{Cu} ($\mu\Omega$ cm) at 295 K	λ_{Cu} (nm) at 295 K
$V_g = +1.2$ V	2.98	670	6.11	380
$V_g = 0$ V	3.11	610	6.36	350
$V_g = -1.5$ V	3.25	410	6.55	300
Change	8.7%	43%	6.9%	23%

Fig. 2(b), and $P_1 = P_2 = P_e$. The low T downturns associated with the Kondo effect are still present.

At 5 K, λ_{Cu} is tuned between 410 nm under $V_g = -1.5$ V and 670 nm under $V_g = +1.2$ V. Using $\lambda_{Cu} = 610$ nm under $V_g = 0$ V as the baseline, 43% tuning of λ_{Cu} is achieved between opposite polarities of V_g. Such large and reversible tunability of λ_{Cu} on demand in metal is unprecedented. The values of ρ_{Cu} and λ_{Cu} under various V_g values at 5 K are summarized in Table I. The opposite trends of tuning for λ_{Cu} and ρ_{Cu} is qualitatively consistent with the Elliott-Yafet (EY) spin relaxation model [35,36], which predicts an inversely proportional relationship between λ_{Cu} and ρ_{Cu} assuming a constant spin-flip probability. The EY model assumes that spin flip events occur with a certain probability upon each momentum scattering event.

The spin current through the Cu channel passing by the spin detector F_2 is $I_s = \frac{1}{2}P_1 I_e e^{-L/\lambda_{Cu}}$. To achieve effective tuning of a robust spin current in a NLSV, the spin transport channel length L should be comparable to the range of λ_{Cu}. If $L \ll \lambda_{Cu}$, the tuning effect of I_s will be minimal. If $L \gg \lambda_{Cu}$, the magnitude of I_s will be minimal. The current NLSV device with $L = 800$ nm matches well with the tuning range 410 nm $\leqslant \lambda_{Cu} \leqslant 670$ nm. The spin current I_s near F_2 is modulated by a factor of 2.1 between $0.013I_e$ and $0.027I_e$ at 5 K. The spin signal ΔR_s, which is the nonlocal electrical voltage resulting from the spin current, is tuned by a factor of 3 as shown in Figs. 1(c)–1(e). The reason for the different tuning factors is that the spin resistance $\rho_{Cu}\lambda_{Cu}/A$ has to be factored in to convert I_s into ΔR_s. Nevertheless, both the spin signal and the spin current in this mesoscopic metallic NLSV are tuned substantially.

IV. TUNING THE KONDO EFFECT

In addition to λ_{Cu} and ρ_{Cu}, the Kondo effect in the Cu channel is tuned by ionic gating as well. The Kondo effect arises from the antiferromagnetic exchange interaction between the localized spin of a magnetic impurity and the delocalized spins of conduction electrons of the host metal. The well-known experimental signature of the Kondo effect in metals is the increase of resistivity (or momentum relaxation rate) at low temperature. The plots of $\rho_{Cu}(T) - \rho_{Cu}(5$ K$)$ versus T between 5 and 22 K under V_g of $+1.2$, 0, and -1.5 V are shown in Fig. 4(a). The curve with $V_g = -1.5$ V shows a pronounced low temperature increase of ρ_{Cu}, revealing the presence of the Kondo effect. The curves with V_g of 0 and $+1.2$ V, however, show no obvious upturn at low temperatures. Apparently, the strength of the Kondo effect at negative V_g is much stronger than that at positive V_g.

For Cu based NLSVs with Py electrodes, it has been shown that Fe impurities in the Cu channel are responsible for the Kondo effect [8,20,21]. Fe and Ni impurities are introduced into the Cu channels unintentionally during the fabrication processes [15,29,37]. Fe impurities in Cu is well known as a Kondo system with a Kondo temperature of $T_K = 30$ K. But T_K for Ni impurities in Cu is above 1000 K and no Kondo features should be present in the temperature range of this study [29,38]. The total ρ_{Cu} can be expressed as

$$\rho_{Cu}(T) = \rho_{def} + \rho_{ph}(T) + \rho_K(T), \qquad (2)$$

where ρ_{def}, ρ_{ph}, and ρ_K are defect, phonon, and Kondo contributions to the resistivity. While ρ_{def} is a constant, phonon resistivity can be approximated as $\rho_{ph}(T) = AT^5$ at low T. The Kondo resistivity can be described by a phenomenological formula [39]

$$\rho_K(T) = \rho_{K0}\left(\frac{T_K'^2}{T^2 + T_K'^2}\right)^s, \qquad (3)$$
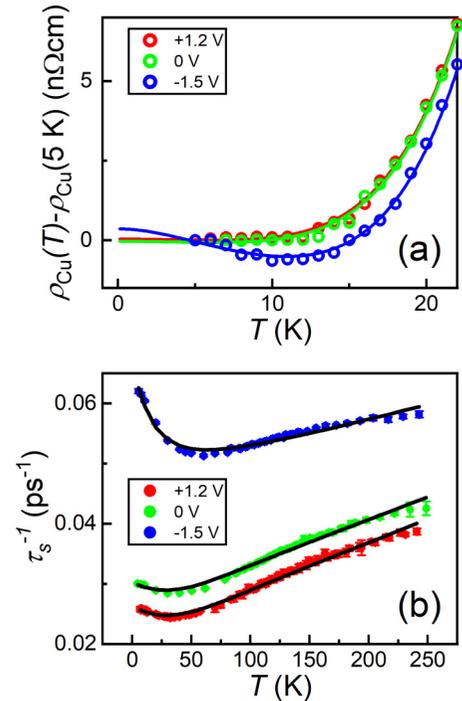
FIG. 4. (a) The plot of $\rho_{Cu}(T) - \rho_{Cu}(5$ K$)$ versus T between 5 and 22 K for the Cu channel under various V_g values. (b) The spin relaxation rate τ_s^{-1} versus T between 5 and 250 K under various V_g values. All solid lines are fitting lines.

TABLE II. Kondo resistivity ρ_{K0}, defect resistivity ρ_{def}, parameter A, Kondo spin flip probability α_K, defect spin flip probability α_{def}, and phonon spin flip probability α_{ph} under various V_g values.

V_g	ρ_{K0} ($\mu\Omega\,cm$)	ρ_{def} ($\mu\Omega\,cm$)	A ($\mu\Omega\,cm\,K^{-5}$)	α_K	α_{def}	α_{ph}
+1.2 V	3.3×10^{-4}	2.98	1.30×10^{-9}	0.40	3.2×10^{-4}	2.7×10^{-4}
0 V	3.4×10^{-4}	3.11	1.30×10^{-9}	0.32	3.7×10^{-4}	2.6×10^{-4}
−1.5 V	4.2×10^{-3}	3.25	1.32×10^{-9}	0.22	5.5×10^{-4}	2.0×10^{-4}

where $T_K' = T_K/\sqrt{2^{1/s} - 1}$, and $s = 0.225$. ρ_{K0} is the Kondo resistivity at $T = 0$ and scales with the Kondo momentum scattering rate. It also represents the strength of the Kondo effect in general. The values of ρ_{K0} under various V_g values are obtained by fitting Eq. (2) to the three curves in Fig. 4(a) and tabulated in Table II. $\rho_{K0} = 4.2 \times 10^{-3}\,\mu\Omega$ cm under $V_g = -1.5$ V is one order of magnitude higher than $\rho_{K0} = 3.3 \times 10^{-4}\,\mu\Omega$ cm under $V_g = +1.2$ V or the value under 0 V, confirming substantial tuning of the Kondo effect strength. The concentration of Fe impurities is proportional to ρ_{K0} [40] and can be conveniently estimated by using an empirical formula that involves the temperature corresponding the resistivity minimum of the $\rho_{Cu}(T)$ curve [15,37,41,42]. For this NSLV, the concertation is <5 ppm and measurements are done at $T \geqslant 5$ K. Therefore, interactions between impurities, which were found at >100 ppm and $T < 0.4$ K [43], can be neglected.

The tuning of the Kondo effect is also reflected in the data of τ_s^{-1} versus T in Fig. 4(b), where τ_s is the spin relaxation time and τ_s^{-1} is the spin relaxation rate of the Cu channel. τ_s is calculated from λ_{Cu} by using relation $\lambda_{Cu} = \sqrt{D\tau_s}$, where $D = \frac{1}{3}v_F^2\tau_e$ is the diffusion constant. $v_F = 1.57 \times 10^6$ m/s is the Fermi velocity of Cu and the momentum relaxation time τ_e can be obtained by using the Drude model $\rho_{Cu} = m/\tau_e ne^2$, where $n = 8.47 \times 10^{28}$ m^{-3} is the Cu electron density, m is the electron mass, and e is the electron charge. All three τ_s^{-1} versus T curves under various V_g values in Fig. 4(b) show upturns at low temperature, which can be attributed to the enhanced spin relaxation rate due to the Kondo effect. The upturn under $V_g = -1.5$ V is clearly more pronounced than those under 0V and $+1.2$ V. This is consistent with the more pronounced resistivity upturn associated with $V_g = -1.5$ V in Fig. 4(a).

The total spin relaxation rate can be expressed as the summation of three individual spin relaxation rates,

$$\frac{1}{\tau_s(T)} = \alpha_{def}\frac{1}{\tau_{e,def}} + \alpha_{ph}\frac{1}{\tau_{e,ph}(T)} + \alpha_K\frac{1}{\tau_{eK}(T)}, \quad (4)$$

where $\tau_{e,def}^{-1}$, $\tau_{e,ph}^{-1}$, and τ_{eK}^{-1} are the electron momentum relaxation rates for defects, phonon, and the Kondo effect, and they are related to ρ_{def}, ρ_{ph}, or ρ_K through the Drude model, respectively. α_{def}, α_{ph}, and α_K are the respective spin-flip probabilities for each momentum scattering type. Data in Fig. 4(b) can be fitted well by Eq. (4). The details of the fitting method are given in our previous work [15]. The fitted values of α_{def}, α_{ph}, and α_K under various V_g values are listed in Table II. The values of α_K are significantly larger than α_{def} or α_{ph} by orders of magnitude. This is due to the antiferromagnetic nature of the Kondo exchange interaction, which leads to a high probability of spin flip at a Kondo momentum

scattering event. The good quality of the fitting corroborates the conclusion from Fig. 4(a) that the strength of the Kondo effect can be tuned by the ionic gating.

V. EVOLUTION OF THE GATING EFFECTS AT ROOM TEMPERATURE

At this point, it is natural to inquire about the origin of the observed tuning effects under ionic gating. The discussion of electrochemical versus electrostatic origins has been an important theme in the literature of the ionic gating technique. Under V_g, positive or negative ions accumulate on the outer surface of the gated material and attract opposite charges on the inner surface forming an electric double layer (EDL). Due to the short distance ($\sim$1 nm) between opposite charges of the EDL, a strong surface electric field (>1 V/nm) and a high surface charge density exceeding 10^{14}/cm^2 can be achieved and are capable of tuning properties of 2D materials, ultra-thin metallic films, and materials with low charge densities. In many previous works, the experimental evidence indeed points to the intense electrostatic field or/and the high charge doping as the origin of the tuning effects. In some cases [21,44–46], however, arguments for a complete or a partial electrochemical origin of the tuning have been presented. Such divergence of opinions highlights the complexity of this versatile ionic gating technique.

Some previous works on ionic gating are relevant to metallic materials and/or spintronics. Tuning of resistivity in Au films has been demonstrated and interpreted as an electrostatic effect that modulates the charge density in metal [23]. However, x-ray absorption near edge structure measurements suggested an electrochemical origin: reversible oxidation of Au films [44]. Tuning of the inverse spin Hall effect, Kondo effect, and ferromagnetism in Pt by ionic gating has been demonstrated as well [47,48]. In the following, by analyzing the evolution of the gating effects at RT, we show that an electrochemical origin is responsible for the tuning effects in Cu based NLSVs.

Clear RT tuning of spin signals is already shown in Figs. 3(c) and 3(d): $\Delta R_s = 2.2$ mΩ under $V_g = +1.2$ V and $\Delta R_s = 1.0$ mΩ under $V_g = -1.5$ V for the NLSV device at 295 K. The spin signal is tuned by a factor of 2.2. However, the initial tuning range of the device is much smaller and the prolonged gating measurements surprisingly amplify the range. To understand the origin of the tuning effects, it is useful to trace the evolution of gating measurements over time. Figure 5(a) shows selected data of ΔR_s and V_g versus the gating measurement time t_g at RT. Figure 5(b) shows selected data of ρ_{Cu} and V_g versus t_g. The t_g timer starts on the initial gating measurement ($t_g = 0$) of the as-fabricated device and continues for any RT gating measurement (either ΔR_s or ρ_{Cu}).
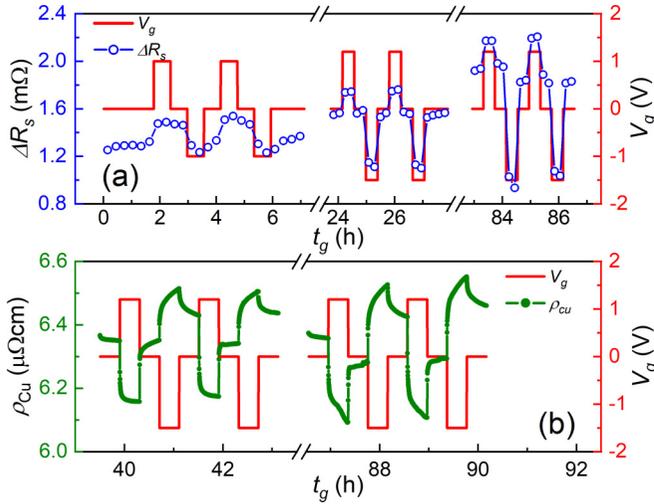
FIG. 5. (a) The measured ΔR_s (left vertical axis) and applied V_g (right vertical axis) as functions of gating time t_g at 295 K. (b) The measured ρ_{Cu} (left vertical axis) and applied V_g (right vertical axis) as a function of t_g at 295 K.

FIG. 6. (a) The tuning range of spin signals $\Delta R_s^+ - \Delta R_s^-$ between positive and negative polarities of V_g for each complete gate cycle as a function of t_g for the NSLV at 295 K. Different symbols indicate the range of applied V_g. (b) Hysteresis loop of ΔR_s versus V_g around $t_g = 12$ h. (c) Hysteresis loop of ΔR_s versus V_g around $t_g = 31$ h.

The timer pauses when the device is cooled below 273 K (upon electrolyte freezing) and resumes once the device is warmed above 273 K. For this device, t_g extends to ∼90 h and the low T measurements shown in the previous section are mainly conducted during the time interval 60 h $< t_g <$ 80 h. The RT measurements shown in Figs. 3(c) and 3(d) are conducted around $t_g = 85$ h.

As shown by the solid lines in Fig. 5, V_g is applied in a square-wave fashion and varies abruptly between zero and two opposite polarities. At each V_g, a few (2–4) data points are available for ΔR_s in Fig. 5(a) but many more data points are available for ρ_{Cu} in Fig. 5(b), because the measurement of each ΔR_s requires sweeping magnetic field and is more time consuming. Clearly Fig. 5(a) shows that the tuning range of ΔR_s increases substantially over time. A moderate increase of tuning range over time is also evident for ρ_{Cu} in Fig. 5(b).

In Fig. 5(a) at $t_g = 0$ h, $\Delta R_s = 1.2$ mΩ is measured under $V_g = 0$ V representing the spin signal of the as-fabricated device. At $t_g = 2$ h, $V_g = +1.0$ V is applied and ΔR_s increases moderately to 1.5 mΩ, which remains even when V_g is reduced to 0 V. ΔR_s returns to 1.2 mΩ under $V_g = -1.0$ V completing the first gate cycle. The tuning features for the next several gate cycles (between $+1.0$ and -1.0 V) are quite similar but the tuning range $\Delta R_s^+ - \Delta R_s^-$ gradually increases, where ΔR_s^+ and ΔR_s^- are the spin signals under the positive and negative V_g, respectively. Figure 6(a) shows $\Delta R_s^+ - \Delta R_s^-$ of each gate cycle versus t_g. In the first five gating cycles during 0 h $< t_g <$ 24 h, the tuning range increases from 0.2 to 0.4 mΩ. During 24 h $< t_g <$ 28 h, there are two gate cycles with V_g between $+1.2$ and -1.5 V and the tuning ranges increase to 0.6 mΩ. The plots of ΔR_s and V_g versus t_g for these two gate cycles are shown in the middle section of Fig. 5(a). Compared to the interval $0 < t_g < 6$ h in the left section of Fig. 5(a), there is less hysteresis in the tuning features: the value of ΔR_s at $V_g = 0$ V following $V_g = +1.2$ V is the same as that following $V_g = -1.5$ V.

The final complete gate cycles are measured during 83 h $< t_g <$ 87 h and the plot of ΔR_s versus t_g data are shown in the right section of Fig. 5(a). The spin signals ΔR_s are 2.2, 1.9, and 1.0 mΩ under V_g of $+1.2$, 0, and -1.5 V, respectively. ΔR_s more than doubles between opposite V_g polarities and the tuning range is 1.2 mΩ. Strikingly, the tuning range increases from merely 0.2 to 1.2 mΩ during 87 h of gate cycling at 295 K as summarized in Fig. 6(a). In addition, as can be seen in Fig. 5(a), the value of ΔR_s at $V_g = 0$ V also increases from 1.2 mΩ in the as-fabricated device to 1.9 mΩ in the same device after 87 h of gate cycling. The evolution of the tuning range and the value of ΔR_s at $V_g = 0$ V over time strongly suggests that the origin of the tuning effects is electrochemical instead of electrostatic.

As mentioned earlier in this section, the hysteresis features of the tuning effect also evolve over time. An explicit hysteresis loop of ΔR_s versus V_g can be obtained when V_g is varied in small steps between two polarities. The loop in Fig. 6(b) is measured between -1.0 and $+1.0$ V around $t_g = 12$ h, and there is an obvious hysteresis. The loop in Fig. 6(c) is measured between -1.2 and $+1.2$ V around $t_g = 31$ h, and there is essentially no hysteresis on the negative side of V_g. Though a small hysteresis remains on the positive side of V_g, ΔR_s values at $V_g = 0$ are almost the same for the upward and downward branches. Such evolution of hysteresis further supports the electrochemical origin.

The evolution of resistivity tuning at 295 K can be examined in Fig. 5(b). During 39 h $< t_g <$ 43 h, ρ_{Cu} is tuned by 5.5% with a lower ρ_{Cu} at $+1.2$ V and a higher ρ_{Cu} at -1.5 V. During 86 h $< t_g <$ 90 h, the tuning range of ρ_{Cu} is enhanced to 6.9%. To quantify the optimized tuning effects, we estimate λ_{Cu} values under various V_g values at 295 K by using ΔR_s data during 83 h $< t_g <$ 87 h as well as ρ_{Cu} data during 87 h $< t_g <$ 90 h. At $+1.2$ V, λ_{Cu} is 380 nm and ρ_{Cu} is 6.11 μΩ cm. At -1.5 V, λ_{Cu} is suppressed to 300 nm and

ρ_{Cu} increases to 6.55 $\mu\Omega$ cm. While λ_{Cu} is tuned by 23% (relative to $\lambda_{Cu} = 350$ nm under $V_g = 0$), ρ_{Cu} is tuned by 6.9% at 295 K. The optimized tuning of λ_{Cu} and ρ_{Cu} at 295 K is summarized in Table I.

VI. DISCUSSION OF POSSIBLE MECHANISMS OF THE TUNING EFFECTS

The identification of the electrochemical origin of the gating effect in our NLSVs is an important revelation, because the controversy of electrostatic versus electrochemical origins has been long standing with the ionic gating method [21,44–46]. Here we further discuss possible underlying electrochemical mechanisms. To pinpoint to an exact mechanism, advanced characterization methods on the morphology and composition of the Cu channels are necessary. However, a direct probe into the mesoscopic Cu channel is very challenging because of the thick layer of solid electrolyte and the delicate nature of the nanoscale NLSVs.

Since the surfaces of the Cu channels are exposed to air and the electrolyte without capping layers, natural oxides form. Recent studies [49,50] show that O^{2-} ions can be moved by an electric field bidirectionally through a GdO_x layer to change the oxidation state of an adjacent metallic magnetic layer. It is reasonable to consider if the O^{2-} ions can be driven by the electric field of the EDL to affect λ_{Cu} and ρ_{Cu}. Because of the short charge screening length (∼0.1 nm) of metal, however, electric field cannot penetrate into the bulk of Cu metal. Therefore, field-driven motion of O^{2-} ions, if any, is only confined to the surface region within one atomic layer. This mechanism is unlikely to be responsible for the observed tuning effects. Another possibility is that the O^{2-} ions may simply diffuse into Cu via the grain boundaries without being driven by a field. However, there is no reason that such diffusion process can be modulated by the gate voltage.

Alternatively, we hypothesize a Li diffusion process via the Cu grain boundaries. The ionic gating voltage can modulate the concentration of Li on the Cu surfaces, thereby controlling the diffusion. Our gating experiment with PEO:LiClO$_4$ electrolyte and Cu films resembles some electrochemical systems used to study Li ion batteries [51]. In these systems, Li^+ containing electrolyte is in contact with a Cu electrode, and a bias voltage with the proper polarity induces concentrated Li^+ ions or even plated Li metal on the Cu surface. Diffusion of Li from the surface into the bulk of the Cu electrode occurs along the grain boundaries [51–54]. When the bias voltage changes sign, the process is reversed and Li moves out of the Cu [51]. Another relevant and similar process is that Li^+ ions can intercalate into layered electrodes of Li ion batteries or layered 2D materials and can be removed by reversing the bias [55–57].

We propose the following scenarios for our system. Under a positive V_g, high concentration of Li is induced on the Cu channel surfaces because of the accumulated Li^+ ions from the electrolyte and/or plated Li metal, and Li diffuses into the channel along the grain boundaries. Note that Cu is inert to Li and does not form intermetallic compounds with Li at room temperature [58]. It is well known that grain boundaries act as potential barriers for conduction electrons and contribute sig-

nificantly to momentum relaxation as well as spin relaxation. As Li atoms fill up the grain boundaries in Cu, these potential barriers are effectively reduced leading to a reduced ρ_{Cu} and an enhanced λ_{Cu}. Under a negative V_g, Li^+ ions or plated Li metal are stripped away from the Cu channel and the surface Li concentration is significantly reduced. Consequently, Li diffuses out of the Cu channel reversing the changes of λ_{Cu} and ρ_{Cu}. The lack of tuning in Al channels, as shown in Figs. 3(a) and 3(b), might be attributed to the uniform Al_2O_3 oxide layer, which blocks the diffusion of Li.

Two main features in Figs. 5 and 6, the gradual increase of the tuning range of ΔR_s and the evolution of its hysteresis, can now be explained in the context of Li diffusion. With repeated bidirectional Li diffusion under gate cycling, the diffusion paths along the grain boundaries become more efficient and the diffusivity for Li increases. At positive V_g, more Li diffuses into the Cu channel. At negative V_g, a greater fraction of the trapped Li in Cu moves out of the channel. Therefore, the tuning range of ΔR_s increases over time. Previous work has shown that Li can reversibly diffuse into and out of Cu with a small amount being trapped [38]. Also because of the enhanced diffusivity, the Li density inside the Cu channel depends more sensitively on the Li concentration at the Cu surfaces. Therefore, the measured ΔR_s responds readily to the applied V_g, which regulates the surface Li concentration, and there is less hysteresis in the ΔR_s versus V_g curve in Fig. 6(c). The exact cause of the enhanced diffusivity is a subject of future study. Possible reasons include cleansing of the grain boundaries via repeated diffusion.

Now we may explain the tuning of the Kondo effect in the context of Li diffusion. Under a positive V_g, concentrated Li atoms accumulate in the Cu grain boundaries. The chemical environment of the Fe impurities, especially those located near the grain boundaries, is profoundly altered from that in a pure Cu host. Therefore, the effectiveness of the antiferromagnetic exchange interaction between the Fe impurity spin and the conduction electron spins is reduced and the Kondo effect is quenched. Under negative V_g, Li moves out of the Cu and Kondo effect is recovered. Note that Li and Fe do not form intermetallic compound [53].

VII. CONCLUSIONS

In conclusion, we demonstrate tuning of spin relaxation length λ_{Cu}, resistivity ρ_{Cu}, and the Kondo effect in Cu thin films by using the ionic gating technique. Polymer electrolyte PEO:LiClO$_4$ is used as the gating medium between a metal gate and the Cu channel of a nonlocal spin valve (NLSV). While the ionic gating can be implemented directly at room temperature, warming and cooling are involved to reset the gate voltage for low temperature gating. At 5 K, the spin signal of a NLSV is modulated by an impressive factor of 3. The value of λ_{Cu} is tuned between 670 and 410 nm and ρ_{Cu} is tuned by 9%. In addition, the strength of the Kondo effect is tuned by one order of magnitude.

At room temperature, λ_{Cu} is tuned reversibly between 380 and 300 nm and ρ_{Cu} is tuned by 7%. The tuning ranges of λ_{Cu} and ρ_{Cu} have been amplified over time by prolonged gating. We conclude that the origin of the tuning effects is electrochemical and is most likely related to reversible diffusion of

Li atoms/ions along Cu grain boundaries. The demonstrated tuning range of λ_{Cu} allows for effective modulation of the spin current in submicron Cu spin transport channels, and opens up the broader potential for tunable metallic spintronic devices.

[1] O. O. Soykal and M. E. Flatte, Phys. Rev. Lett. **104**, 077202 (2010).

[2] C. M. Hu, Phys. Can. **72**, 76 (2016).

[3] J. Grollier, D. Querlioz, K. Y. Camsari, K. Everschor-Sitte, S. Fukami, and M. D. Stiles, Nat. Electron. **3**, 360 (2020).

[4] S. Datta and B. Das, Appl. Phys. Lett. **56**, 665 (1990).

[5] H. C. Koo, J. H. Kwon, J. Eom, J. Chang, S. H. Han, and M. Johnson, Science **325**, 1515 (2009).

[6] J. Bass and W. P. Pratt, J. Phys.: Condens. Matter. **19**, 183201 (2007).

[7] B. Huang, D. J. Monsma, and I. Appelbaum, Phys. Rev. Lett. **99**, 177209 (2007).

[8] T. S. Ghiasi, J. Ingla-Aynes, A. A. Kaverzin, and B. J. van Wees, Nano Lett. **17**, 7528 (2017).

[9] L. A. Benitez, J. F. Sierra, W. S. Torres, A. Arrighi, F. Bonell, M. V. Costache, and S. O. Valenzuela, Nat. Phys. **14**, 303 (2018).

[10] J. S. Xu, T. C. Zhu, Y. K. Luo, Y. M. Lu, and R. K. Kawakami, Phys. Rev. Lett. **121**, 127703 (2018).

[11] A. Avsar, J. Y. Tan, M. Kurpas, M. Gmitra, K. Watanabe, T. Taniguchi, J. Fabian, and B. Ozyilmaz, Nat. Phys. **13**, 888 (2017).

[12] M. Johnson and R. H. Silsbee, Phys. Rev. Lett. **55**, 1790 (1985).

[13] F. J. Jedema, A. T. Filip, and B. J. van Wees, Nature (London) **410**, 345 (2001).

[14] Y. Fukuma, L. Wang, H. Idzuchi, S. Takahashi, S. Maekawa, and Y. Otani, Nat. Mater. **10**, 527 (2011).

[15] X. Y. Shen and Y. Ji, Phys Rev B **104**, 085101 (2021).

[16] H. Shimotani, H. Asanuma, A. Tsukazaki, A. Ohtomo, M. Kawasaki, and Y. Iwasa, Appl. Phys. Lett. **91**, 082106 (2007).

[17] K. Ueno, S. Nakamura, H. Shimotani, A. Ohtomo, N. Kimura, T. Nojima, H. Aoki, Y. Iwasa, and M. Kawasaki, Nat. Mater. **7**, 855 (2008).

[18] A. S. Dhoot, C. Israel, X. Moya, N. D. Mathur, and R. H. Friend, Phys. Rev. Lett. **102**, 136402 (2009).

[19] D. Braga, I. G. Lezama, H. Berger, and A. F. Morpurgo, Nano Lett. **12**, 5218 (2012).

[20] A. Das, S. Pisana, B. Chakraborty, S. Piscanec, S. K. Saha, U. V. Waghmare, K. S. Novoselov, H. R. Krishnamurthy, A. K. Geim, A. C. Ferrari, and A. K. Sood, Nat. Nanotechnol. **3**, 210 (2008).

[21] J. Jeong, N. Aetukuri, T. Graf, T. D. Schladt, M. G. Samant, and S. S. P. Parkin, Science **339**, 1402 (2013).

[22] J. T. Ye, Y. J. Zhang, R. Akashi, M. S. Bahramy, R. Arita, and Y. Iwasa, Science **338**, 1193 (2012).

[23] D. Daghero, F. Paolucci, A. Sola, M. Tortello, G. A. Ummarino, M. Agosto, R. S. Gonnelli, J. R. Nair, and C. Gerbaldi, Phys. Rev. Lett. **108**, 066807 (2012).

[24] T. Kimura, T. Sato, and Y. Otani, Phys. Rev. Lett. **100**, 066602 (2008).

[25] Y. J. Cai, Y. M. Luo, C. Zhou, C. Qin, S. H. Chen, Y. Z. Wu, and Y. Ji, J. Phys. D: Appl. Phys. **49**, 185003 (2016).

[26] D. K. Efetov and P. Kim, Phys. Rev. Lett. **105**, 256805 (2010).

[27] X. J. Wang, H. Zou, L. E. Ocola, and Y. Ji, Appl. Phys. Lett. **95**, 022519 (2009).

[28] M. Johnson, Phys. Rev. Lett. **70**, 2142 (1993).

[29] L. O'Brien, M. J. Erickson, D. Spivak, H. Ambaye, R. J. Goyette, V. Lauter, P. A. Crowell, and C. Leighton, Nat. Commun. **5**, 3927 (2014).

[30] J. D. Watts, L. O'Brien, J. S. Jeong, K. A. Mkhoyan, P. A. Crowell, and C. Leighton, Phys. Rev. Materials **3**, 124409 (2019).

[31] C. H. Shang, J. Nowak, R. Jansen, and J. S. Moodera, Phys. Rev. B **58**, R2917 (1998).

[32] D. T. Pierce, R. J. Celotta, J. Unguris, and H. C. Siegmann, Phys. Rev. B **26**, 2566 (1982).

[33] D. Mauri, D. Scholl, H. C. Siegmann, and E. Kay, Phys. Rev. Lett. **61**, 758 (1988).

[34] Y. J. Cai, C. Qin, F. Kandaz, X. Y. Shen, C. Zhou, M. W. Jia, Y. M. Luo, Y. Z. Wu, and Y. Ji, Phys. Rev. B **100**, 144419 (2019).

[35] R. J. Elliott, Phys. Rev. **96**, 266 (1954).

[36] Y. Yafet, Phys. Lett. A **98**, 287 (1983).

[37] L. O'Brien, D. Spivak, J. S. Jeong, K. A. Mkhoyan, P. A. Crowell, and C. Leighton, Phys. Rev. B **93**, 014413 (2016).

[38] P. A. Schroeder, R. Wolf, and J. A. Woollam, Phys. Rev. **138**, A105 (1965).

[39] D. Goldhaber-Gordon, J. Gores, M. A. Kastner, H. Shtrikman, D. Mahalu, and U. Meirav, Phys. Rev. Lett. **81**, 5225 (1998).

[40] K. W. Kim, L. O'Brien, P. A. Crowell, C. Leighton, and M. D. Stiles, Phys. Rev. B **95**, 104404 (2017).

[41] J. P. Franck, D. L. Martin, and F. D. Manchester, Proc. R. Soc. London, Ser. A **263**, 494 (1961).

[42] J. T. Batley, M. C. Rosamond, M. Ali, E. H. Linfield, G. Burnell, and B. J. Hickey, Phys. Rev. B **92**, 220420(R) (2015).

[43] E. C. Hirschkoff, M. R. Shanabarger, O. G. Symko, and J. C. Wheatley, J. Low Temp. Phys. **5**, 545 (1971).

[44] T. A. Petach, M. Lee, R. C. Davis, A. Mehta, and D. Goldhaber-Gordon, Phys. Rev. B **90**, 081108(R) (2014).

[45] J. Walter, H. L. Wang, B. Luo, C. D. Frisbie, and C. Leighton, ACS Nano **10**, 7799 (2016).

[46] B. Cui, P. Werner, T. P. Ma, X. Y. Zhong, Z. C. Wang, J. M. Taylor, Y. C. Zhuang, and S. S. P. Parkin, Nat. Commun. **9**, 3055 (2018).

[47] S. Dushenko, M. Hokazono, K. Nakamura, Y. Ando, T. Shinjo, and M. Shiraishi, Nat. Commun. **9**, 3118 (2018).

[48] L. Liang, Q. H. Chen, J. M. Lu, W. Talsma, J. Shan, G. R. Blake, T. T. M. Palstra, and J. T. Ye, Sci. Adv. **4**, eaar2030 (2018).

[49] L. Baldrati, A. J. Tan, M. Mann, R. Bertacco, and G. S. D. Beach, App. Phys. Lett. **110**, 012404 (2017).

[50] M. Huang, A. J. Tan, M. Mann, U. Bauer, R. Ouedraogo, and G. S. D. Beach, Sci. Rep. **7**, 7452 (2017).

[51] S. S. Lv, T. Verhallen, A. Vasileiadis, F. Ooms, Y. L. Xu, Z. L. Li, Z. C. Li, and M. Wagemaker, Nat. Commun. **9**, 2152 (2018).

[52] B. J. Neudecker, N. J. Dudney, and J. B. Bates, J. Electrochem. Soc. **147**, 517 (2000).

[53] R. Rupp, B. Caerts, A. Vantomme, J. Fransaer, and A. Vlad, J. Phys. Chem. Lett. **10**, 5206 (2019).

[54] D. Rehnlund, J. Pettersson, K. Edstrom, and L. Nyholm, Chemistryselect **3**, 2311 (2018).

[55] M. S. Whittingham, Chem. Rev. **104**, 4271 (2004).

[56] Y. J. Yu, F. Y. Yang, X. F. Lu, Y. J. Yan, Y. H. Cho, L. G. Ma, X. H. Niu, S. Kim, Y. W. Son, D. L. Feng, S. Y. Li, S. W. Cheong, X. H. Chen, and Y. B. Zhang, Nat. Nanotechnol. **10**, 270 (2015).

[57] M. Rajapakse, B. Karki, U. O. Abu, S. Pishgar, M. R. K. Musa, S. M. S. Riyadh, M. Yu, G. Sumanasekera, and J. B. Jasinski, npj 2D Mater. Appl. **5**, 30 (2021).

[58] H. Okamoto, J. Phase Equilib. Diffus. **32**, 172 (2011).